

# Crystal structure of *Escherichia coli* CyaY protein reveals a previously unidentified fold for the evolutionarily conserved frataxin family

Seung-Je Cho, Myong Gyong Lee, Jin Kuk Yang, Jae Young Lee, Hyun Kyu Song, and Se Won Suh\*

Department of Chemistry, Seoul National University, Seoul 151-742, Korea

Communicated by David S. Eisenberg, University of California, Los Angeles, CA, June 12, 2000 (received for review May 5, 2000)

Friedreich ataxia is an autosomal recessive neurodegenerative disease caused by defects in the *FRDA* gene, which encodes a mitochondrial protein called frataxin. Frataxin is evolutionarily conserved, with homologs identified in mammals, worms, yeast, and bacteria. The CyaY proteins of  $\gamma$ -purple bacteria are believed to be closely related to the ancestor of frataxin. In this study, we have determined the crystal structure of the CyaY protein from *Escherichia coli* at 1.4-Å resolution. It reveals a protein fold consisting of a six-stranded antiparallel  $\beta$ -sheet flanked on one side by two  $\alpha$ -helices. This fold is likely to be shared by all members of the conserved frataxin family. This study also provides a framework for the interpretation of disease-associated mutations in frataxin and for understanding the possible functions of this protein family.

Friedreich ataxia (FRDA), an autosomal recessive neurodegenerative disease, is the most common hereditary ataxia with an estimated prevalence of approximately 1 in 50,000 and a deduced carrier rate of higher than 1 in 110 in European populations (1). FRDA is caused by defects in the *FRDA* gene (also called  $\chi$ 25 gene) on chromosome 9q, which encodes a 210-residue precursor protein called frataxin (2) with a mitochondrial targeting sequence at the N terminus (3). Frataxin deficiency is in most cases (>95%) a consequence of homozygosity for an expanded GAA triplet repeat in the first intron of the *FRDA* gene (2). The expansion results in reduction of the *FRDA* mRNA level in affected individuals (4, 5). A small group (<5%) of patients with FRDA are compound heterozygotes for the GAA expansion on one allele and carry a point mutation within the *FRDA* gene on the other allele. The most common disease-causing missense mutation in frataxin is I154F. This mutation on one allele, together with the hyperexpansion on the other allele, is indistinguishable from typical FRDA in disease severity (2). Other mutations such as L106S, D122Y, and G130V, compounded with hyperexpansive allele, are associated with a milder and more slowly progressive disease course (6, 7).

Frataxin shows a remarkable evolutionary conservation, with homologs present in mammals, *Caenorhabditis elegans*, yeast, and Gram-negative bacteria. Significant similarity between the C-terminal portion of frataxin (residues 90–210) and the CyaY proteins of  $\gamma$ -purple bacteria (Fig. 1) implied that the *FRDA* gene evolved from a *CyaY* gene of the mitochondrial ancestor. Mitochondrial localization of frataxin, initially suggested by its sequence similarity to the CyaY proteins (9), was confirmed experimentally (4). Disruption of the *FRDA* homolog in yeast, *Yfh1*, resulted in accumulation of iron in mitochondria and deficiency in Fe-S–dependent respiratory enzymes and aconitase (10). The neurodegeneration observed in FRDA is believed to be the result of mitochondrial iron accumulation and oxidative stress (11). It has been also observed that the frataxin family bears limited sequence homology to a bacterial protein family, which confers resistance to tellurium (12). Amino acid sequences of the frataxin family members do not show any significant similarity to

proteins of known three-dimensional structure. Recently, a nuclear magnetic resonance assignment of the C-terminal domain of frataxin has been reported (13). To provide structural data on the frataxin protein family, we have determined the three-dimensional structure of the *E. coli* CyaY protein. It reveals a protein fold, which is likely to be shared by other members of the evolutionarily conserved frataxin family (9). The structure also provides a framework for the interpretation of disease-related mutations in frataxin and for designing mutagenesis studies to elucidate possible functions of the members of the frataxin family.

## Materials and Methods

**Crystallization, Data Collection, and Phasing.** Overexpression, purification, and crystallization of the *E. coli* CyaY protein with a six-histidine tag at the C terminus were reported elsewhere (14). The dynamic light scattering analysis was performed with a Model DynaPro-801 instrument from Protein Solutions (Charlottesville, VA) as described (15).

Collection of the native X-ray diffraction to 1.8-Å resolution at 296 K was reported elsewhere (14). CyaY crystallized in the trigonal space group P3<sub>1</sub>21 (or its enantiomorph P3<sub>2</sub>21), with unit cell dimensions of  $a = b = 44.66$  Å and  $c = 99.87$  Å. [The latter space group was determined to be correct during phasing by multiple isomorphous replacement (MIR) on the basis of the handedness of  $\alpha$ -helices.] There is one molecule of the recombinant CyaY per asymmetric unit. For the MIR phase determination, three heavy atom derivatives were prepared by soaking crystals in a solution containing 5 mM HgCl<sub>2</sub> (for 56 days), 10 mM KAu(CN)<sub>2</sub> (for 6 days), and 50 mM (CH<sub>3</sub>)<sub>3</sub>Pb(CH<sub>3</sub>COO) (for 28 days). X-ray data from heavy atom derivatives were collected on an Enraf-Nonius Service (Bohemia, NY) FAST area detector system (Table 1). Mercury sites were located by interpreting the difference Patterson map with the RSPS program (16), and heavy atoms of other derivatives were located in the cross-phased difference Fourier maps. The MIR phases were calculated to 2.5-Å resolution with the program SHARP (17) and were extended to 2.0 Å by density modification with SOLOMON (16).

**Model Building and Refinement.** The resultant electron density map was of sufficient quality to allow tracing the whole polypeptide chain. The model was built with the program O (18) and refined by several cycles of torsion angle dynamics simulated annealing

Abbreviations: FRDA, Friedreich ataxia; MIR, multiple isomorphous replacement.

Data deposition: The atomic coordinates have been deposited in the Protein Data Bank, www.rcsb.org (PDB ID code 1EW4).

\*To whom reprint requests should be addressed. E-mail: sewonsuh@snu.ac.kr.

The publication costs of this article were defrayed in part by page charge payment. This article must therefore be hereby marked "advertisement" in accordance with 18 U.S.C. §1734 solely to indicate this fact.

Article published online before print: *Proc. Natl. Acad. Sci. USA*, 10.1073/pnas.160270897.  
Article and publication date are at www.pnas.org/cgi/doi/10.1073/pnas.160270897

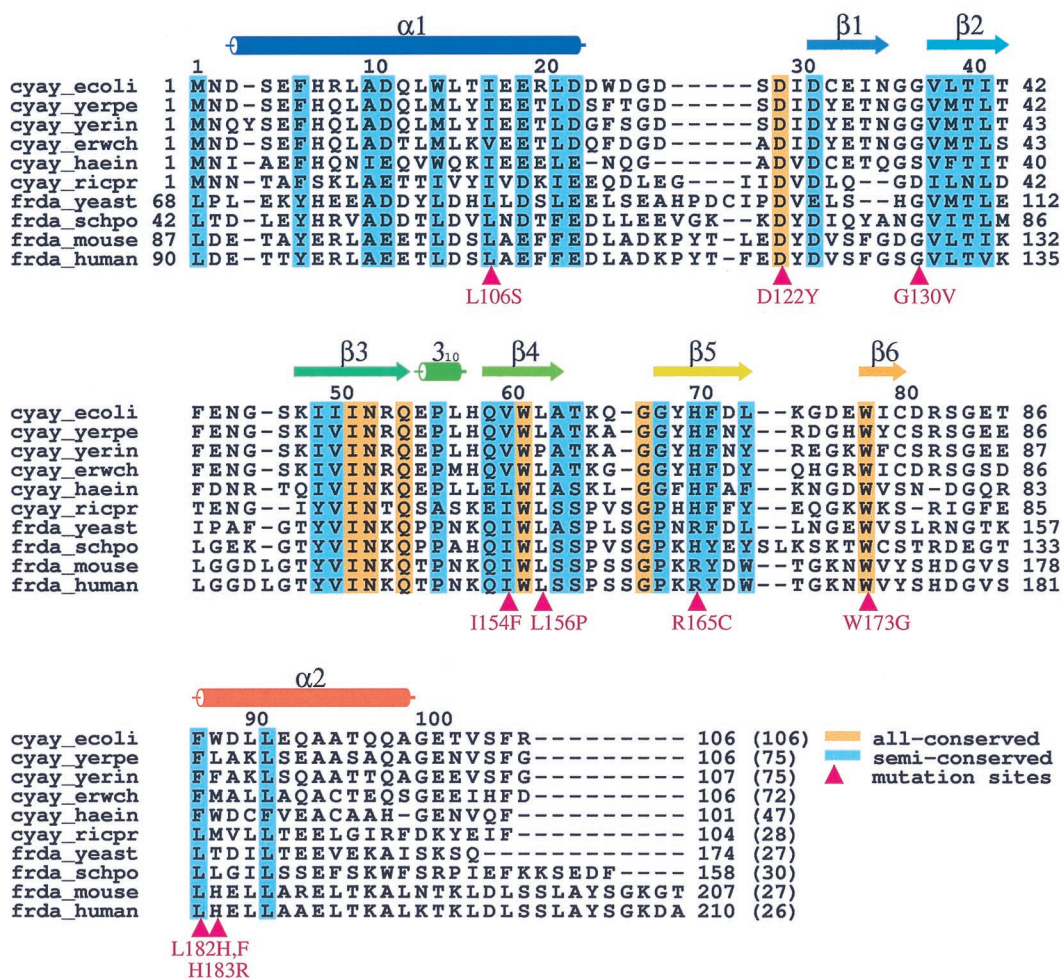


**Fig. 1.** Sequence alignment of 10 members of frataxin family: CyaY/frataxin from *Escherichia coli*, *Yersinia pestis*, *Yersinia intermedia*, *Erwinia chrysanthemi*, *Haemophilus influenzae*, *Rickettsia prowazekii*, *Saccharomyces cerevisiae* (budding yeast), *Schizosaccharomyces pombe*, *Mus musculus* (mouse), and *Homo sapiens* (human). Residues conserved in all sequences are highlighted in gold, and semi-conserved residues are highlighted in cyan. The number of identical residues compared with *E. coli* CyaY is given in parentheses. The disease-associated mutations in frataxin are marked by magenta triangles. Secondary structure elements are indicated above the sequence for *E. coli* CyaY. This figure was produced with ALSCRIPT (8).

followed by positional refinement with a maximum likelihood target function with the CNS program (19), including the bulk solvent correction. Throughout the model building and refinement process, 10% of the reflections were set aside to monitor the  $R_{\text{free}}$  value (20). The initial model had  $R_{\text{work}}$  of 37.6% and  $R_{\text{free}}$  of 42.0% for 20.0- to 2.0-Å data (native 1 in Table 1). The model has been refined to  $R_{\text{work}}$  of 18.9% and  $R_{\text{free}}$  of 21.9% against 20.0- to 1.8-Å data (native 1 in Table 1). At this stage, higher resolution data to 1.4 Å were collected at 100 K by using a Sakabe Weissenberg camera of Photon Factory beamline BL-6B (ref. 21; native 2 in Table 1), with unit cell parameters of  $a = b = 44.18$  Å and  $c = 98.29$  Å. The model has been refined further to  $R_{\text{work}}$  of 18.8% and  $R_{\text{free}}$  of 21.3% against 20.0- to 1.4-Å data (native 2 in Table 1). The refined model accounts for all 106 residues of CyaY and 122 water molecules. Electron density is clear for all parts of the protein except the histidine tag. The stereochemistry of the refined model as assessed by PROCHECK (22) is excellent. Refinement statistics are summarized in Table 1.

## Results and Discussion

**Overall Fold.** We have determined the crystal structure of *E. coli* CyaY at 1.4-Å resolution by MIR based on three heavy atom derivatives (Table 1). There is no indication of the CyaY

protein forming a tight oligomer in the crystal. This result is in agreement with the result of dynamic light scattering analysis, which indicates that the recombinant CyaY protein exists largely as a monomer. The structure of CyaY protein from *E. coli* is prolate, with approximate dimensions of  $45 \times 30 \times 25$  Å<sup>3</sup>. It comprises of a twisted antiparallel  $\beta$ -sheet formed by six consecutive  $\beta$ -strands ( $\beta$ 1– $\beta$ 6), flanked on one side by a long N-terminal  $\alpha$ -helix ( $\alpha$ 1) and a shorter C-terminal  $\alpha$ -helix ( $\alpha$ 2; Fig. 2 Upper). The connections between regular secondary structure elements are short, except a loop after helix  $\alpha$ 1, another loop after strand  $\beta$ 6, and a  $3_{10}$ -helix between strands  $\beta$ 3 and  $\beta$ 4. In the CyaY structure, aromatic and aliphatic side chains of the following residues contribute to the formation of a hydrophobic core: Phe-6, Ala-10, Leu-13, Trp-14, Ile-17, Leu-21, Ile-30, Leu-39, Ile-41, Phe-43, Ile-49, Ile-51, Val-60, Leu-62, Phe-71, Trp-78, Phe-87, Leu-90, Leu-91, Ala-94, Ala-95, Val-103, and Phe-105. No cavity is detected in CyaY with the program GRASP (25). A topology diagram of the secondary structure elements is shown in Fig. 2 Lower. The  $\beta$ -sheet of CyaY has a topology of +1, +1, +1, +1, and +1. Surprisingly, a search for overall structural similarities against the DALI database (26) failed to reveal any significant matches. This result indicates that the *E. coli* CyaY protein adopts a previously unidentified fold.

**Table 1. Crystallographic summary**

	Native 1	HgCl <sub>2</sub>	KAu(CN) <sub>2</sub>	(CH <sub>3</sub> ) <sub>3</sub> Pb(CH <sub>3</sub> COO)	Native 2
Data collection and phasing					
Resolution limit, Å	1.8	2.0	2.2	2.0	1.4
Unique reflections/redundancy	10,309/12.5	7,035/8.2	6,128/3.5	7,844/2.7	22,616/9.1
Completeness, %	92.8 (99.5)*	86.7 (99.2)	98.3 (98.2)	94.7 (77.2)	99.9 (99.4)
R <sub>sym</sub> , % <sup>†</sup>	6.0 (14.4)	10.2 (20.9)	4.2 (8.1)	4.8 (13.5)	4.1 (39.9)
R <sub>iso</sub> , % <sup>‡</sup>	—	47.8 (55.1)	32.9 (36.6)	33.0 (39.6)	—
Phasing (15–2.5 Å, native 1 data)					
Phasing power <sup>§</sup> , centric/acentric	—	2.01/2.83	1.70/2.07	1.26/1.44	—
R <sub>Cullis</sub> , % <sup>¶</sup> , centric/acentric	—	0.55/0.52	0.58/0.62	0.73/0.75	—
Figure of merit <sup>  </sup>	0.79 (0.83 after density modification for 15–2.0 Å data)				
Refinement (20–1.4 Å, native 2 data)					
R <sub>work</sub> /R <sub>free</sub> , %**		18.8/21.3			
Number of reflections		17,535 (working set)/1,944 (test set)			
Number of atoms		863 (in residues 1–106)/122 (water)			
Average B factors, Å <sup>2</sup>		16.9 (main chain)/22.1 (side chain)/30.7 (water)			
rms deviations, bond lengths, Å/bond angles, degrees		0.011/1.46			
Ramachandran plot, %		93.6 (most favored)/6.4 (additionally allowed)			

\*Highest resolution shell given in parentheses.

<sup>†</sup>R<sub>sym</sub> =  $\sum_h \sum_i |I(h,i) - \langle I(h) \rangle| / \sum_h \sum_i I(h,i)$ , where  $I(h,i)$  is the intensity of the  $i$ th measurement of reflection  $h$  and  $\langle I(h) \rangle$  is the average value of  $I(h)$  for all  $i$  measurements.

<sup>‡</sup>R<sub>iso</sub> =  $\sum ||F_{PH}| - |F_P|| / \sum |F_P|$ , where  $F_{PH}$  and  $F_P$  are derivative and native structure factors, respectively.

<sup>§</sup>Phasing power =  $\langle F_H \rangle / E$ , where  $\langle F_H \rangle$  is the rms heavy atom structure factor and  $E$  is the residual lack of closure error.

<sup>¶</sup>R<sub>Cullis</sub> =  $\sum ||F_{PH} \pm F_P| - |F_{PH(calc)}|| / \sum |F_{PH} - F_P|$ .

<sup>||</sup>Figure of merit =  $|\sum P(\alpha)e^{i\alpha} / \sum P(\alpha)|$ , where  $P(\alpha)$  is the phase probability distribution and  $\alpha$  is the phase.

\*\*R<sub>work</sub> and R<sub>free</sub> =  $\sum ||F_o| - |F_c|| / \sum |F_o|$  for the working set and test set (10%) of reflections.

**Sequence Homologs and Conserved Residues.** The *E. coli* CyaY protein shows significant sequence similarity with the C-terminal part of eukaryotic frataxin homologs (Fig. 1). The sequence identity is 24.5% between *E. coli* CyaY and frataxin (residues 90–210) and 26.4% between CyaY and Yfh1p (residues 68–174). This level of identity suggests that the newly discovered fold of CyaY is likely to be shared by frataxins. Among *E. coli* CyaY, Yfh1p, and frataxin, there are 17 invariant residues: Ala-10 ( $\alpha$ 1), Asp-31 ( $\beta$ 1), Gly-37, Val-38 ( $\beta$ 2), Thr-40 ( $\beta$ 2), Ile-51 ( $\beta$ 3), Asn-52 ( $\beta$ 3), Gln-54 ( $\beta$ 3), Pro-56 ( $\beta$ 3), Gln-59 ( $\beta$ 4), Trp-61 ( $\beta$ 4), Leu-62 ( $\beta$ 4), Gly-67, Asp-72 ( $\beta$ 5), Trp-78 ( $\beta$ 6), Gly-84, and Leu-91 ( $\alpha$ 2). It is apparent that the residues in  $\beta$ -strands, particularly  $\beta$ 3 and  $\beta$ 4, are more strongly conserved than those in the two  $\alpha$ -helices. Gly-37, Gly-67, and Gly-84 are located in  $\beta$ -turns between  $\beta$ 1 and  $\beta$ 2,  $\beta$ 4 and  $\beta$ 5, as well as  $\beta$ 6 and  $\alpha$ 2, respectively. Of these 17 residues, only four (Ile-51, Leu-62, Trp-78, and Leu-91) are involved in forming the hydrophobic core. When the sequence alignment is expanded to 10 members of the frataxin family (Fig. 1), seven residues are invariant: Asp-31, Ile-51, Asn-52, Gln-54, Trp-61, Gly-67, and Trp-78. Ile-51 and Trp-78 are part of the hydrophobic core. The remaining five residues are exposed to the solvent and are clustered on one face of the structure (Fig. 3). A surface patch defined by these residues (Fig. 4 *Left*) may play a crucial role in protein–protein interactions, which may be required for still poorly understood biological functions.

**Disease-Associated Missense Mutations.** Known disease-causing missense mutations in frataxin include L106S, D122Y, G130V, I154F, L156P, R165C, W173G, L182H, L182F, and H183R (7, 27, 28). They correspond to Ile-17, Asp-29, Gly-37, Val-60, Leu-62, His-70, Trp-78, Phe-87, and Trp-88 of CyaY (Fig. 1). Of these, Ile-17, Val-60, Leu-62, Trp-78, and Phe-87 contribute to the hydrophobic core (Fig. 3). It seems reasonable to expect that the missense mutations of the equivalent residues in frataxin may disturb the proper formation of its hydrophobic core and may

cause an alteration of its three-dimensional structure or of its misfolding. Gly-37 of CyaY is highly conserved among frataxin family members, and an inspection of the aligned amino acid sequences in Fig. 1 indicates that at least one glycine is present at this position or right next to it. Thus, it is reasonable to expect that mutation of this glycine to valine in human frataxin will not only affect the loop conformation of this region but will also expose a hydrophobic side chain onto the protein surface (Fig. 4 *Left* and *Center*). This mutation may influence possible protein–protein interactions involving frataxin. The two mutation sites Asp-29 and Trp-78 are invariant among 10 sequences aligned in Fig. 1. Asp-29 of CyaY is located near the start of strand  $\beta$ 1 (Fig. 3). Substitution of the corresponding Asp-122 in frataxin with tyrosine will expose a neutral side chain, which is bulkier and more hydrophobic. This change may adversely influence the surface characteristics of frataxin (Fig. 4 *Left*) and may also affect its interaction with other proteins. His-70 is fully exposed to the solvent on the  $\beta$ -sheet side of CyaY (Fig. 4 *Left*). The corresponding mutation R165C of frataxin will result in a substantial alteration of the surface property. H183R mutation in frataxin corresponding to the partially exposed Trp-88 of CyaY lies on the  $\alpha$ -helix face in proximity to the C terminus of CyaY (Fig. 4 *Right*). The surface feature of this face is likely to be much different between CyaY and frataxin because of the C-terminal extension in frataxin. It is not clear from the CyaY structure why FRDA associated with I154F should be more severe than that attributed to other mutations. It could be related to other still uncharacterized but critical roles of Ile-154, for example, in *in vivo* folding. It is also worth mentioning that the corresponding residue in CyaY, Val-60, is adjacent to the invariant Trp-61 not only in terms of sequence but also in the spatial arrangement of the side chains. The aromatic ring of this highly conserved Trp-61 is fully exposed to the solvent (Figs. 3 and 4), suggesting a critical role in its interaction with other proteins or possibly the lipid membrane.

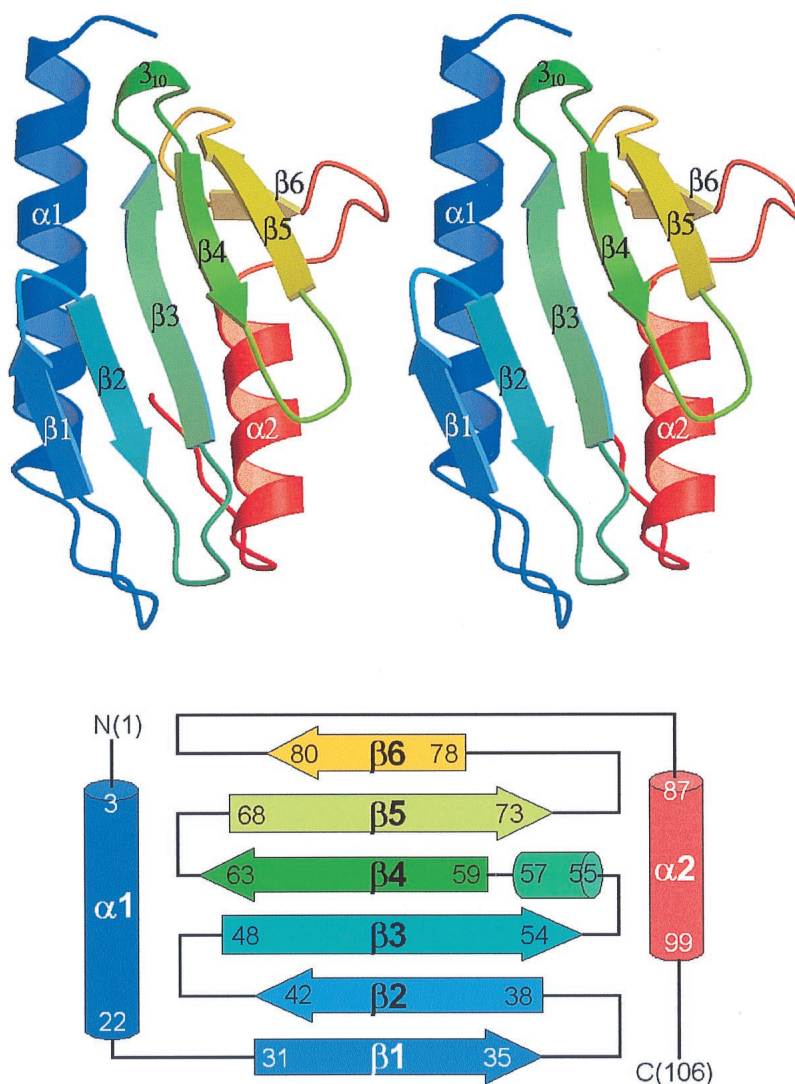


**Fig. 2.** Overall fold of *E. coli* CyaY. (Upper) Stereo ribbon diagram showing the secondary structure elements. Six  $\beta$ -strands (arrows), two  $\alpha$ -helices (ribbons), and a  $3_{10}$ -helix are drawn and labeled. MOLSCRIPT (23) and RASTER3D (24) programs were used to generate the figure. (Lower) Topology diagram.

**Conserved Surface Features for Shared Biological Functions.** It was proposed that the yeast frataxin homolog Yfh1p maintains mitochondrial iron homeostasis both directly, by promoting iron export, and indirectly, by regulating iron levels, and therefore mitochondrial intermediate peptidase activity, which promotes mitochondrial iron uptake (29). A knockout study of the *CyaY* gene in *E. coli* suggested, however, that CyaY affects neither intracellular iron level nor resistance to exogenous oxidants (30). It was conjectured that the bacterial CyaY proteins and the eukaryotic frataxin homologs may serve related functions but may differ in the carrier system that they activate or the metabolite that they bind (30).

CyaY is a very acidic protein, with a calculated pI of 4.2. Similarly, the C-terminal fragments of Yfh1p (residues 68–174) and human frataxin (residues 90–210) have very low calculated pIs of 4.5 and 4.6, respectively. Interestingly, the charge distribution in the CyaY structure is highly asymmetric, with no negative charge on the  $\beta$ -sheet side (Fig. 4 *Center* and *Right*). This side is also rich in the evolutionarily conserved residues (Figs. 3 and 4 *Left*). This structural feature is highly significant, suggesting that the  $\beta$ -sheet of *E. coli* CyaY, with

conserved residues on the surface, is likely to be involved in protein–protein interactions that may be crucial for its biological functions. This observation implies that the *E. coli* CyaY protein may also function as a regulatory protein, as suggested for frataxin or its yeast homolog.

**Database Search for Possible Functions.** Two structural databases were queried for similar residue constellation in CyaY and any protein of known structure and function. None of the active site templates in the PROCAT database (31) of functional groups in enzyme active sites matches any constellation of residues in the CyaY structure. This result is consistent with the absence in the CyaY structure of a deep cleft or a pocket, which is a salient feature of an enzyme active site. In view of the possibility that eukaryotic frataxin homologs undergo a conformational change on binding  $Fe^{2+}$  itself or a protein sensor of the  $Fe^{2+}$  level in mitochondria in regulating the iron efflux, the most notable result of a search for the presence of a known protein motif by RIGOR (32) is a putative  $Fe^{3+}$  binding site formed by His-7, Glu-55, and His-58. However, these residues are not highly conserved in other members of the

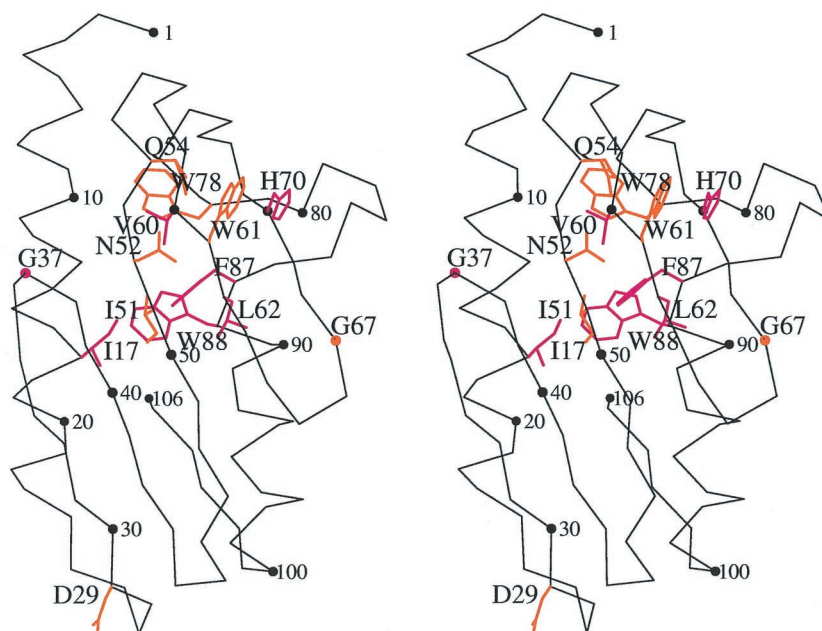


**Fig. 3.** Stereo C $\alpha$  diagram showing the conserved residues (side chains in gold) and the residues corresponding to the disease-associated mutations in frataxin (side chains in magenta).

frataxin family, and experimental data do not support a high-affinity binding of metal ions. Metal analysis of the purified *E. coli* CyaY protein by inductively coupled plasma atomic emission spectrometry could not detect any bound metal ions (Mg, V, Cr, Mn, Fe, Co, Ni, Cu, Zn, or Mo), and there is no indication of bound metal ions in the electron density. However, a possibility remains that different amino acids could be involved in iron binding by other members of the frataxin family.

### Conclusions

Unexpectedly, the crystal structure of *E. coli* CyaY reported in this article has revealed a previously unidentified protein fold for the evolutionarily conserved frataxin family. This fold of

the *E. coli* CyaY protein makes it difficult to gain insight into possible functions of the frataxin family members through a structural comparison. Nevertheless, the distribution of conserved residues in the CyaY structure suggests that the bacterial CyaY proteins and the eukaryotic frataxin homologs may share common biological functions, which are likely to be mediated by the protein-protein interactions through the negative charge-deficient  $\beta$ -sheet side of the structure. This study should also stimulate further mutagenesis and biochemical studies for dissecting possible functions of the frataxin family. The initial set of mutagenesis targets may include the invariant surface residues Asp-31, Asn-52, Gln-54, Trp-61, and Gly-67.

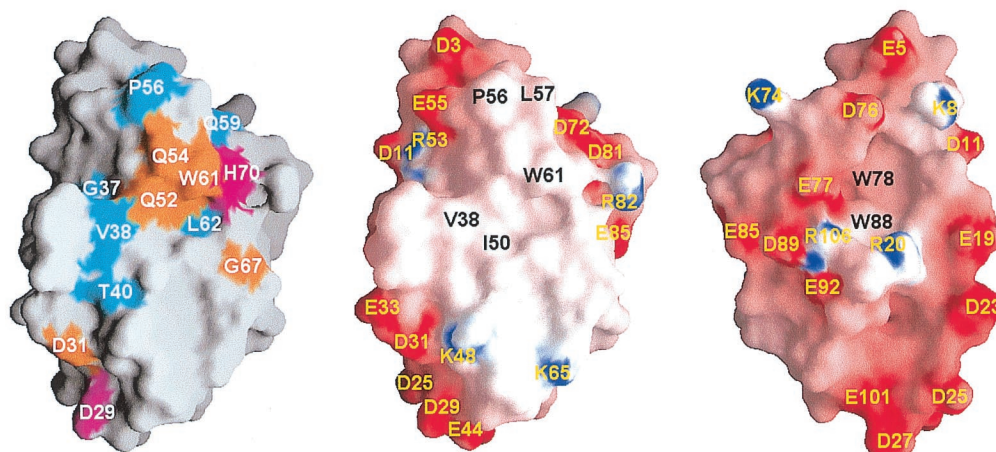


**Fig. 4.** Surface representation of *E. coli* CyaY. (Left) Strictly conserved residues (gold), semiconserved residues (cyan), and residues corresponding to disease-associated mutations in frataxin (magenta) are indicated. This view is the same as that in Figs. 2 and 3 Left. (Center) Diagram showing the electrostatic potential at the molecular surface of the  $\beta$ -sheet side of *E. coli* CyaY in the same orientation as in Left. The surface is color-coded according to the potential: red,  $-15$  kT; white,  $0$  kT; and blue  $+15$  kT. (Right) A view obtained by a  $180^\circ$  rotation of Center around a vertical axis. This figure was drawn with GRASP (25).

We thank Dr. N. Sakabe, Dr. M. Suzuki, and Dr. N. Igarashi for assistance during data collection at BL-6B of Photon Factory, Japan. We also thank the InterUniversity Center for Natural Science Research Facilities, Seoul National University, for providing the x-ray equipment.

This work was supported by the Korea Science and Engineering Foundation through the Center for Molecular Catalysis and by the Brain Korea 21 program. M.G.L. and J.K.Y. are recipients of the Brain Korea 21 fellowship.

1. Delatycki, M. B., Williamson, R. & Forrest, S. M. (2000) *J. Med. Genet.* **37**, 1–8.
2. Campuzano, V., Montermini, L., Moltò, M. D., Pianese, L., Cossée, M., Cavalcanti, F., Monros, E., Rodius, F., Duclos, F., Monticelli, A., *et al.* (1996) *Science* **271**, 1423–1427.
3. Gordon, D. M., Shi, Q., Dancis, A. & Pain, D. (1999) *Hum. Mol. Genet.* **8**, 2255–2262.
4. Campuzano, V., Montermini, L., Lutz, Y., Cova, L., Hindelang, C., Jiraerspong, S., Trottier, Y., Kish, S. J., Faucheux, B., Trouillas, P., *et al.* (1997) *Hum. Mol. Genet.* **6**, 1771–1780.
5. Bidichandani, S. I., Ashizawa, T. & Patel, P. (1998) *Am. J. Hum. Genet.* **62**, 111–121.
6. Bidichandani, S. I., Ashizawa, T. & Patel, P. I. (1997) *Am. J. Hum. Genet.* **60**, 1251–1256.
7. Bartolo, B., Mendell, J. R. & Prior, T. W. (1998) *Am. J. Med. Genet.* **79**, 396–399.
8. Barton, G. J. (1993) *Protein Eng.* **6**, 37–40.
9. Gibson, T. J., Koonin, E. V., Musco, G., Pastore, A. & Bork, P. (1996) *Trends Neurosci.* **19**, 465–468.
10. Rötig, A., de Lonlay, P., Chretien, D., Foury, F., Koenig, M., Sidi, D., Munnich, A. & Rustin, P. (1997) *Nat. Genet.* **17**, 215–217.
11. Delatycki, M. B., Camakaris, J., Brooks, H., Evans-Whipp, T., Thorburn, D. R., Williamson, R. & Forrest, S. M. (1999) *Ann. Neurol.* **45**, 673–675.
12. Foury, F. (1999) *FEBS Lett.* **456**, 281–284.
13. Musco, G., de Tommasi, T., Stier, G., Kolmerer, B., Bottomley, M., Adinolfi, S., Muskett, F. W., Gibson, T. J., Frenkiel, T. A. & Pastore, A. (1999) *J. Biomol. NMR* **15**, 87–88.
14. Lee, M. G., Cho, S., Yang, J. K., Song, H. K. & Suh, S. W. (2000) *Acta Crystallogr. D* **56**, 920–921.
15. Lee, M. G., Lee, J. Y., Song, H. K. & Suh, S. W. (1999) *Acta Crystallogr. D* **55**, 1219–1221.
16. Collaborative Computational Project Number 4 (1994) *Acta Crystallogr. D* **50**, 760–763.
17. de la Fortelle, E. & Bricogne, G. (1997) *Methods Enzymol.* **276**, 472–494.
18. Jones, T. A., Zou, J.-Y., Cowan, S. W. & Kjeldgaard, M. (1991) *Acta Crystallogr. A* **47**, 110–119.
19. Brünger, A. T., Adams, P. D., Clore, G. M., DeLano, W. L., Gros, P., Grosse-Kunstleve, R. W., Jiang, J. S., Kuszewski, J., Nilges, M., Pannu, N. S., *et al.* (1998) *Acta Crystallogr. D* **54**, 905–921.
20. Brünger, A. T. (1992) *Nature (London)* **355**, 472–475.
21. Sakabe, K., Sasaki, K., Watanabe, N., Suzuki, M., Wang, Z. G., Miyahara, J. & Sakabe, N. (1997) *J. Synchrotron Radiat.* **4**, 136–146.
22. Laskowski, R. A., MacArthur, M. W., Moss, D. S. & Thornton, J. M. (1993) *J. Appl. Crystallogr.* **26**, 283–291.
23. Kraulis, P. J. (1991) *J. Appl. Crystallogr.* **24**, 946–950.
24. Merritt, E. A. & Bacon, J. A. (1997) *Methods Enzymol.* **277**, 505–524.
25. Nicholls, A., Sharp, K. A. & Honig, B. (1991) *Proteins* **11**, 281–296.
26. Holm, L. & Sander, C. D. (1998) *Nucleic Acids Res.* **26**, 316–319.
27. Forrest, S. M., Knight, M., Delatycki, M. B., Paris, D., Williamson, R., King, J., Yeung, L., Nassif, N. & Nicholson, G. A. (1998) *Neurogenetics* **1**, 253–257.
28. Cossée, M., Durr, A., Schmitt, M., Dahl, N., Trouillas, P., Allinson, P., Kostrzewa, M., Nivelon-Chevallier, A., Gustavson, K. H., Kohlschütter, A., *et al.* (1999) *Ann. Neurol.* **45**, 200–206.
29. Branda, S. S., Yang, Z. Y., Chew, A. & Isaya, G. (1999) *Hum. Mol. Genet.* **8**, 1099–1110.
30. Li, D. S., Ohshima, K., Jiralerspong, S., Bojanowski, M. W. & Pandolfo, M. (1999) *FEBS Lett.* **456**, 13–16.
31. Wallace, A. C., Borkakoti, N. & Thornton, J. M. (1997) *Protein Sci.* **6**, 2308–2323.
32. Kleywegt, G. J. (1999) *J. Mol. Biol.* **285**, 1887–1897.